

Supplementary information

Micron-Sized Fe-Cu-Si Ternary Composite Anodes for High Energy Li-ion Batteries

Sujong Chae[‡], Minseong Ko[‡], Seungkyu Park, Namhyung Kim, Jiyoung Ma and Jaephil Cho*

School of Energy and Chemical Engineering, Ulsan National Institute of Science and Technology (UNIST), Ulsan, 689-798, South Korea.

[‡] These authors contributed equally.

MATERIALS AND METHODS

Preparation of FeCuSi: The amorphous Si nanoparticles were prepared through decomposition of monosilane (SiH_4) gas at 400 °C. As a first step, 3.5 g of amorphous Si nanoparticles were well dispersed in 0.6 L of distilled water. Then, 7 g of iron nitrate nonahydrate ($\text{Fe}(\text{NO}_3)_3 \cdot 9\text{H}_2\text{O}$, Aldrich) and 2 g of copper nitrate trihydrate ($\text{Cu}(\text{NO}_3)_2 \cdot 3\text{H}_2\text{O}$, Aldrich) were added. Under stirring, the mixed solution was then atomized and dried through spray dryer (Mini Spray Dryer B-290, BUCHI Labortechnik) at 200 °C of inlet temperature. Afterwards, spray dried particles were simply heated in a tube furnace at various temperatures and 1 hour of duration time under hydrogen atmosphere.

Material characterization: FeCuSi was investigated with scanning electron microscopy (SEM, Verios 460, FEI), focused ion beam (FIB, Quanta 3D FEG), and X-ray diffraction (XRD, D/MAZX 2500V/PC, Rigaku). In addition, high resolution transmission electron microscopy (HR-TEM, JEM-2100F, JEOL) was utilized for detailed characterization, where sample preparation was carried out using dual-beam focused ion beam (FIB, Helios 450HP, FEI). Statistical analysis for size distribution of FeCuSi was performed with laser diffraction particle size analysis instrument (Microtrac S3500, Microtrac). Tap density was measured by density analyser (GeoPyc 1360, micromeritics) with 1 g of each sample. Specific surface area and pore size distribution were analysed through BET and BJH methods, respectively, with surface area and porosity analyzer (TriStar II, micromeritics). The change of electrode thickness at the lithiation state were measured with micrometer after disassembling coin cells in Ar-filled glove box. The change was estimated with the equation:

$$\frac{(\text{Electrode thickness at Nth cycle} - \text{Electrode thickness at 1st cycle})}{\text{Electrode thickness at 1st cycle}} \times 100(\%)$$

Electrochemical characterization

1) Anode materials in half-cell: The electrode was fabricated with active material (FeCuSi, C-SiO_x, and FeSi₂, respectively), carbon black (Super P, TIMCAL), carboxymethyl cellulose (CMC), and styrene butadiene rubber (SBR) with the mass ratio of 80:10:5:5. The homogeneously blended slurry was coated on copper foil with ~1mg/cm² of loading level, dried at 80 °C for 30 minutes, and then went through vacuum drying at 110 °C for 2 hours without calendaring. The electrochemical properties were measured at 25 °C with 2032R coin-type using metallic Li foil as a counter electrode. All the cells were assembled in Argon-filled glove box. Microporous polyethylene, and 1.3 M LiPF₆ in ethylene carbonate (EC)/ethyl methyl carbonate (EMC)/ diethyl carbonate (DEC) (=3/5/2, v/v/v) with 10% fluoroethylene carbonate (FEC) and 0.5% vinylene carbonate (VC) (Panax Starlyte) were used as separator and electrolyte, respectively.

The half-cells were run with constant current (CC) – constant voltage (CV) mode between 0.005 and 1.5 V for the formation cycle and between 0.005 and 1 V for the cycling test with TOSCAT-3100 battery cycler (TOYO SYSTEM). The rate was 0.1C for the formation cycle and 0.5C for the cycling test, while constant voltage was at 0.005V with 13 mA/g, 11 mA/g and 17 mA/g cut off for FeCuSi, C-SiO_x, and FeSi₂, respectively. (1C was set as 1.3 A/g, 1.1 A/g and 1.7 A/g for FeCuSi, C-SiO_x, and FeSi₂, respectively.)

2) Graphite-blended anodes in half-cell: FeCuSi, C-SiO_x, and FeSi₂ were blended with natural graphite (BTR) to obtain 420 mAh/g of specific capacity with 7wt%, 5wt%, and 9wt%, respectively. The electrode was fabricated with active materials composed of Si-based materials and graphite, CMC and SBR with the mass ratio of 97:1.5:1.5 as minimized contents of binding materials. The homogeneously blended slurry was coated on copper foil with 8.5 mg/cm² of loading level which corresponds to 3.44~3.48 mAh/cm², dried at 80 °C for 30 minutes, and then went through vacuum drying at 110 °C for 2 hours with calendaring in order to increase the electrode density up to 1.6 g/cc. The electrochemical properties were measured at 25 °C with 2032R coin-type using Li foil as a counter electrode. The cell assembly and other battery components except anodes were the same with those in above electrochemical characterization.

The half-cells were run with CC-CV mode between 0.005 and 1.5 V for the formation cycle and between 0.005 to 1 V for the cycling test with TOSCAT-3100 battery cycler (TOYO SYSTEM). The rate was 0.1C

for the formation cycle and 0.5C for the cycling test, while constant voltage was at 0.005V with 4.2 mA/g cut off. (1C was set as 0.42 A/g for all half-cells).

3) LiCoO₂ in half-cell: The electrode was fabricated with LiCoO₂, carbon black (Super P, TIMCAL), and polyvinylidene fluoride (PVDF) with the mass ratio of 94:3:3. The homogeneously blended slurry was coated on aluminium foil with 20.4 mg/cm² of loading level which corresponds to ~3.42 mAh/cm², dried at 110 °C for 1 hour. Afterwards, the electrode was calendared in order to increase the electrode density up to 3.6 g/cc. The electrochemical properties were measured at 25 °C with 2032R coin-type using Li foil as a counter electrode. All the cells were assembled in Argon-filled glove box. Separator and electrolytes were the same with those of anodes in half-cell.

The half-cells were run with CC-CV mode between 3.0 and 4.45 V with TOSCAT-3100 battery cycler (TOYO SYSTEM). The rate was 0.1C for the formation cycle and 0.5C for the cycling test, while constant voltage was at 4.45 V with 3.6 mA/g cut off. (1C was set as 0.18 A/g.)

4) Full-cells with graphite-blended anodes and LiCoO₂: The electrodes of graphite-blended anodes and LiCoO₂ for half-cell test were identically utilized for full-cell system. The N.P ratio was estimated as 1.11 to 1.14. The electrochemical properties were measured at 25 °C with 2032R coin-type. All the cells were assembled in Argon-filled glove box. Separator and electrolytes were the same with those of others.

The full-cells were run with CC-CV mode between 2.5 to 4.35 V with TOSCAT-3100 battery cycler (TOYO SYSTEM). The rate was 0.1C for the formation cycle with constant voltage at 4.35V and 0.03mA/cm² cut off. In the cycling test, 0.5C and 1C were set as charging and discharging rate, respectively, while constant voltage was at 4.35 V with 0.06 mA/cm² cut off. (1C was set as 3.0 mA/cm².)

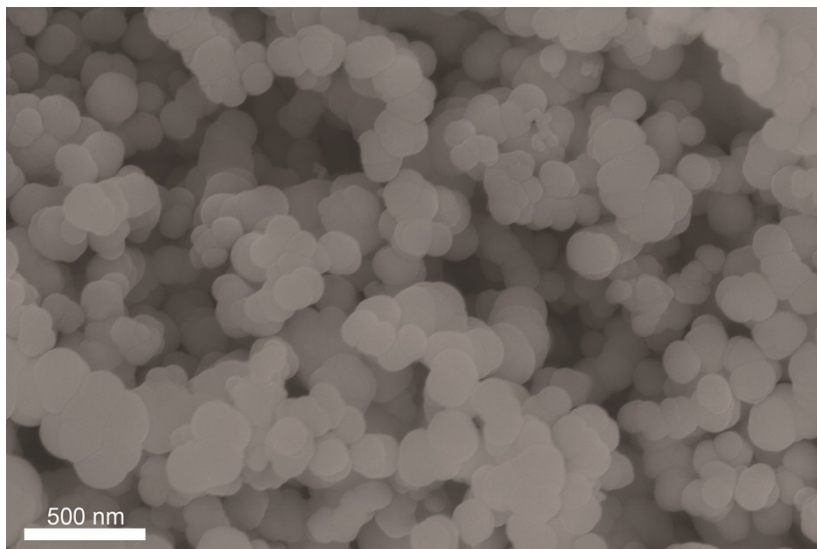


Figure S1. SEM image of amorphous silicon nanoparticles which were synthesized through chemical vapor deposition (CVD) of monosilane (SiH_4).

No.	Index	2 θ (deg)
Fe		
1	(011)	44.64
2	(002)	65.04
Cu		
1	(111)	43.40
2	(002)	50.40
3	(022)	74.06
Si		
1	(111)	28.40
2	(022)	47.26
3	(113)	56.06
4	(004)	69.04
5	(133)	76.32
FeSi ₂		
1	(001)	17.20
2	(011)	37.62
3	(110)	47.64
4	(012)	48.90
5	(111)	51.02
6	(003)	53.44
7	(013)	64.36
8	(020)	69.70
9	(021)	72.46
10	(004)	73.64
11	(113)	74.42
Cu _{3.17} Si		
1	(110)	43.40
2	(103)	50.40
3	(023)	74.06

Table S1. The peak list of Fe, Cu, Si, FeSi₂, and Cu_{3.17}Si with the index from the XRD analysis. The references of Fe, Cu, Si, FeSi₂, and Cu_{3.17}Si are ICSD 631729, 627117, 43403, 24360, 160694, respectively.

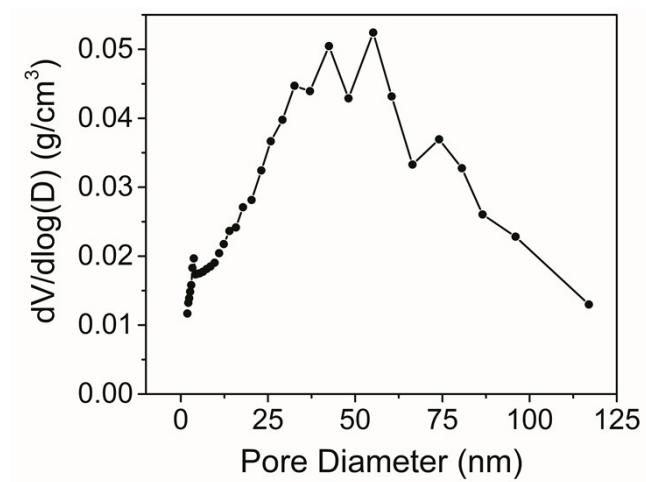


Figure S2. Pore size distribution of FeCuSi. The derivative volume with respect to the pore diameter shows where clusters of pores of a particular diameter occur.

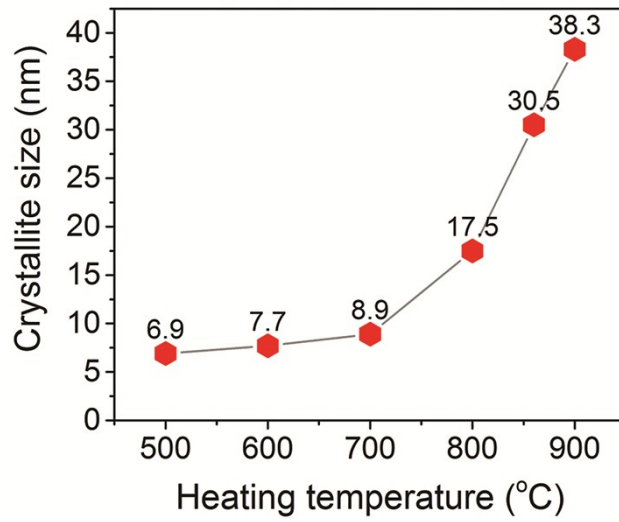


Figure S3. Crystallite sizes of FeCuSi with different heating temperatures.

Crystallite sizes of FeCuSi as a function of heating temperature were estimated with the Halder-Wagner method in PDXL software (Rigaku).

$$\left(\frac{\beta}{\tan \theta}\right)^2 = \frac{K\lambda}{L} \cdot \frac{\beta}{\tan \theta \sin \theta} + 16e^2$$

β = integral breadth

K = shape factor

λ = wave length of the X - ray

L = crystallite size

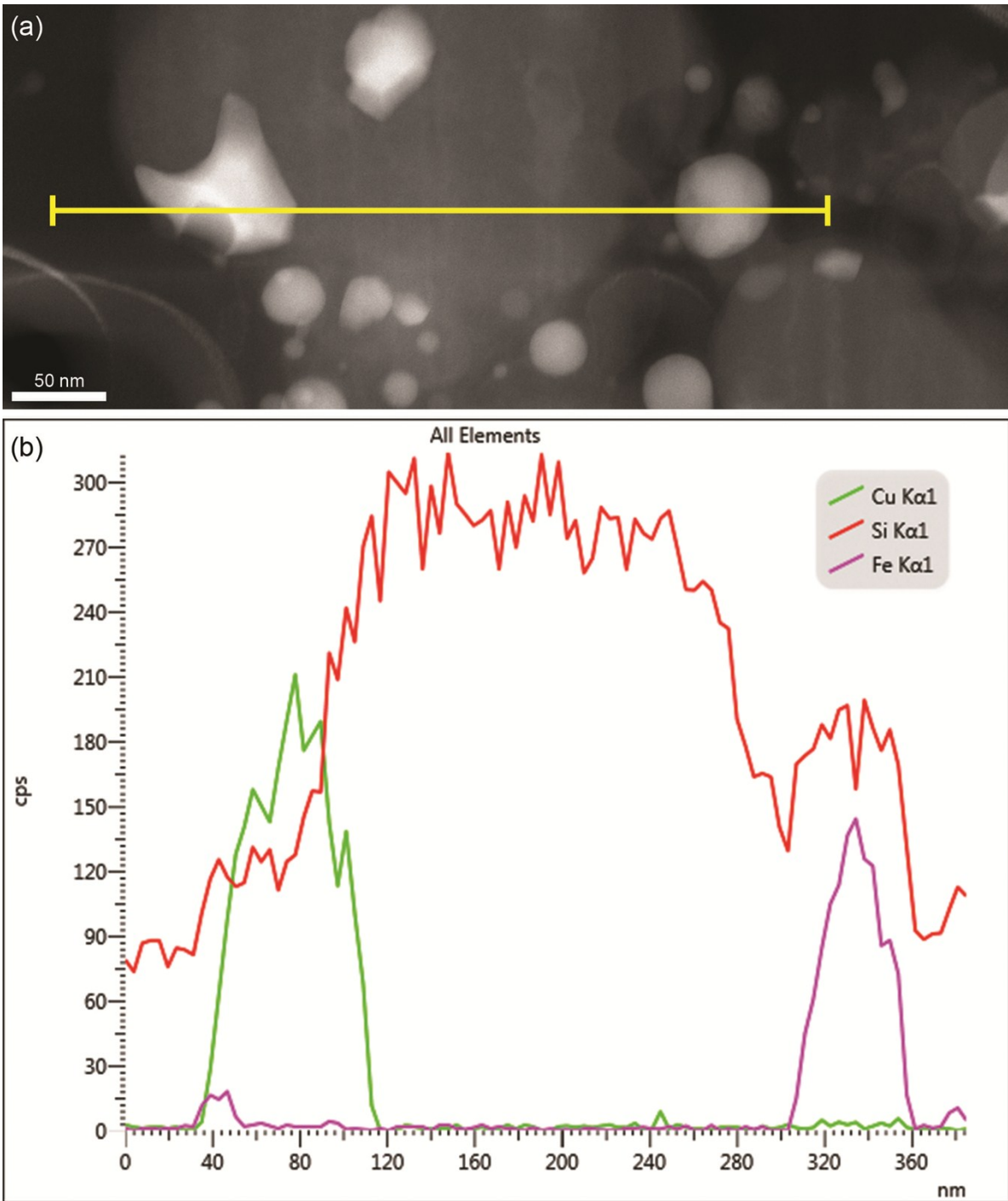


Figure S4. EDS line scan of FeCuSi. (a) Magnified HAADF-STEM image of FeCuSi. (b) Element profile according to line scanning in (a).

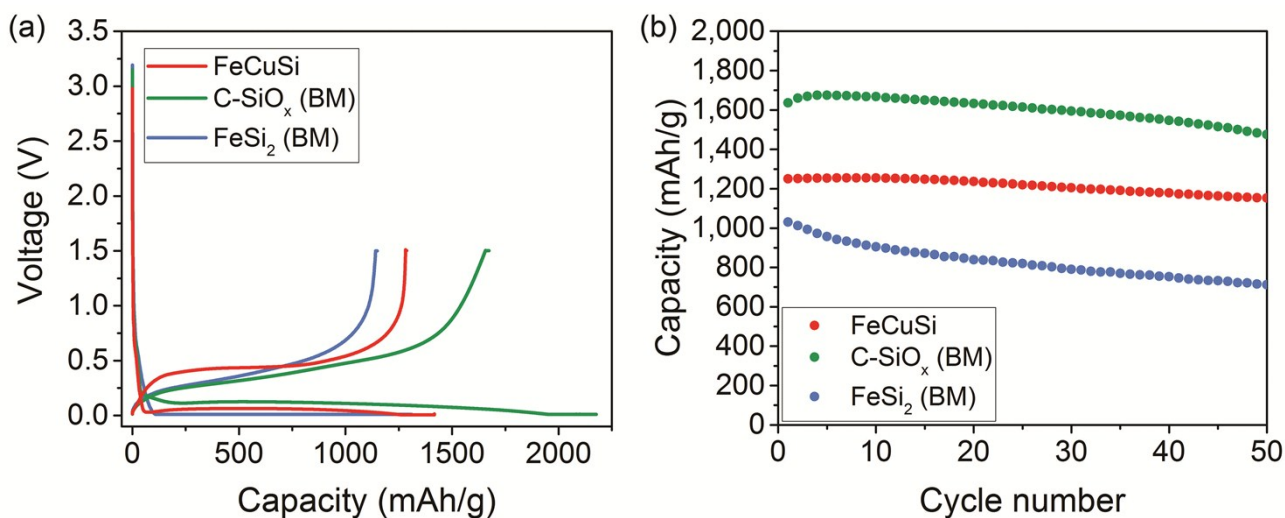


Figure S5. Electrochemical characterization of FeCuSi with benchmarking samples in half-cell. (a)

Voltage profiles of FeCuSi, C-SiO_x, and FeSi₂ at the formation cycle. (b) Reversible capacities of FeCuSi, C-SiO_x, and FeSi₂ for 50 cycles. The formation cycle (a) and cycling test (b) were carried out at a rate of 0.1C and 0.5C, respectively. (1C was set as 1.3 A/g, 1.1 A/g and 1.7 A/g for FeCuSi, C-SiO_x, and FeSi₂, respectively.) All electrochemical tests were performed at 25 °C in 2032R coin-type cell.

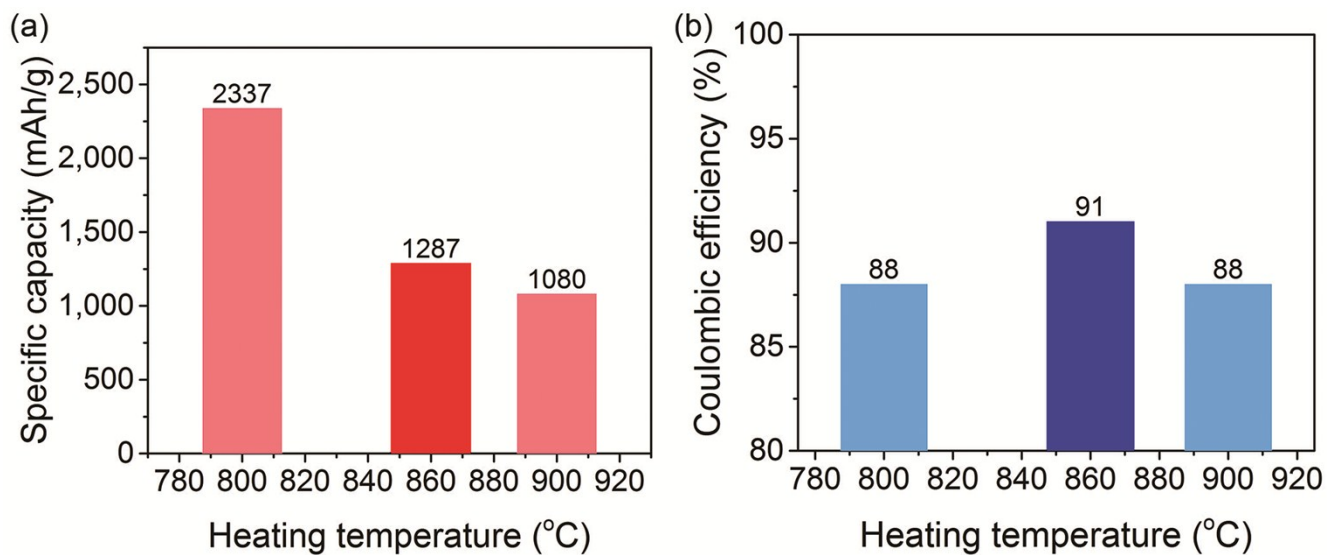


Figure S6. Optimization for heating temperature of FeCuSi. (a) Reversible capacities of FeCuSi as a function of heating temperature. (b) Coulombic efficiencies of FeCuSi with diverse heating temperature. FeCuSi with 860 °C of heating temperature was optimized one.

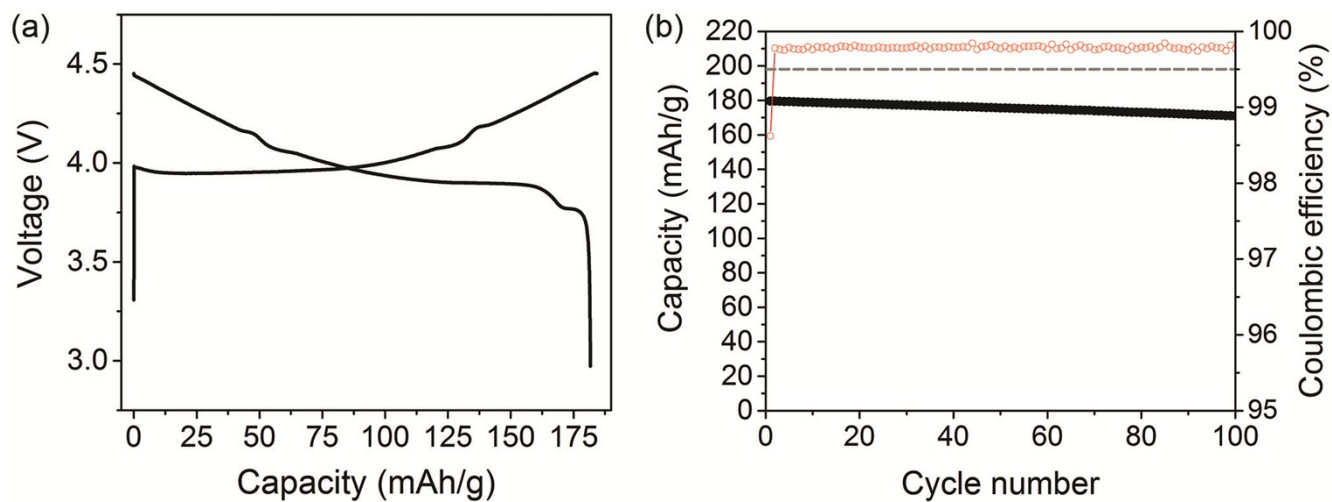


Figure S7. Electrochemical properties of LCO. (a) Voltage profile of LCO at the formation cycle. (b) Reversible capacities of LCO for 100 cycles with 0.5C. The formation cycle (a) and cycling test (b) were carried out at a rate of 0.1C and 0.5C, respectively. (1C = 0.18 A/g) All electrochemical test were performed at 25 °C in 2032R coin-type cell.

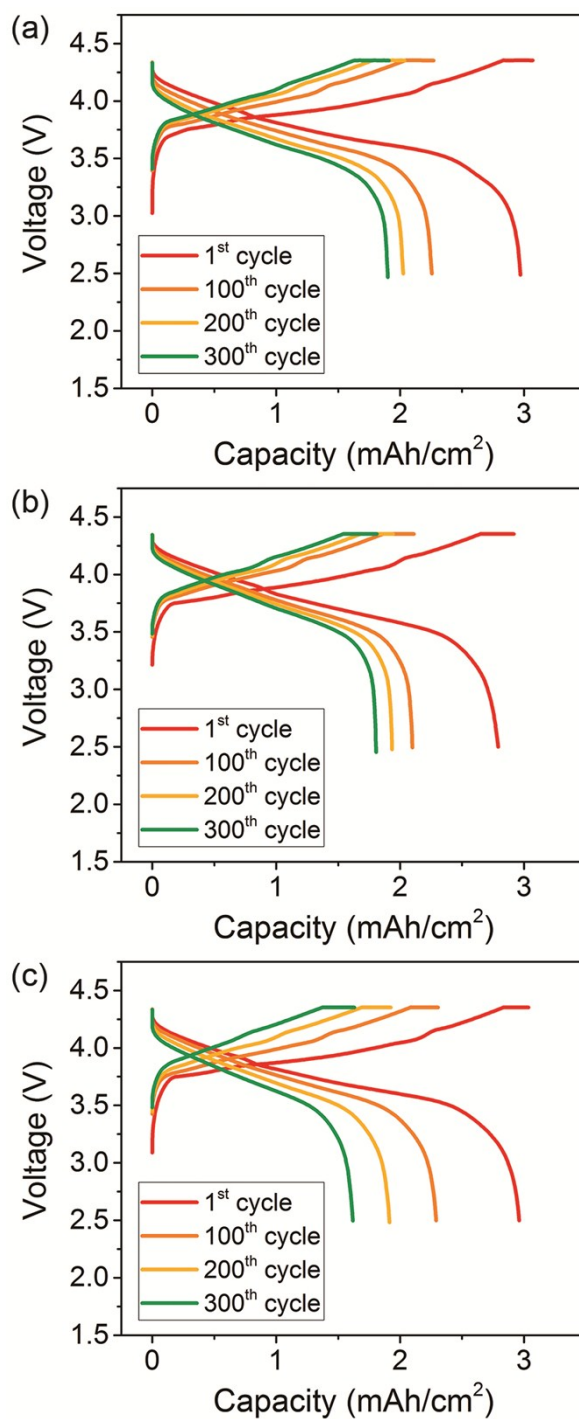


Figure S8. Various voltage profiles of FeCuSi (a), C-SiO_x (b), and FeSi₂ (c) plotted for 1st, 100th, 200th, and 300th cycle.